69th International Astronautical Congress (IAC), Bremen, Germany, 1-5 October 2018.
Copyright © 2018 by Andrea Colagrossi. Published by the International Astronautical Federation with permission.

IAC–18–C1.3.8

CISLUNAR NON-KEPLERIAN ORBITS RENDEZVOUS & DOCKING: 6DOF GUIDANCE AND CONTROL

Andrea Colagrossi[a*], Michèle Lavagna[b]

[a] Ph.D. Candidate. Department of Aerospace Science and Technology, Politecnico di Milano, Via La Masa 34, 20156 Milano - Italy, andrea.colagrossi@polimi.it.
[b] Associate Professor. Department of Aerospace Science and Technology, Politecnico di Milano, Via La Masa 34, 20156 Milano - Italy, michelle.lavagna@polimi.it.
[*] Corresponding Author

Abstract

Future science and exploration missions are supposed to exploit cislunar environment as effective outpost to advance technology readiness in view of human presence beyond Earth. These ambitious space programmes entail modular large space infrastructures to be available in non-Keplerian orbits, in the Moon vicinity, to run manned and robotic activities. The latter in preparation of a safe and reliable operational environment for humans to come. As ISS operations teach, in space outposts ask for complex logistic, which leans on rendezvous and docking/undocking capabilities between space segments and embrace different engineering disciplines. So far, no mission performed autonomous and accurate proximity operations but in LEO. Conversely, several flown missions were operational on non-Keplerian orbits, exploiting the increased knowledge about n-body dynamics modelling for trajectory design. However, existing studies deeply investigating the 6DOF relative dynamics in non-Keplerian orbits are somewhat missing; this area of investigation is now mandatory to support the cislunar infrastructure design and implementation, assessing and addressing practical solutions for GNC strategies, which shall be applicable to reliably manage proximity operations of the lunar gateway. In this direction, the paper discusses and justifies the 6DOF model, based on circular restricted and full ephemeris models, implemented to analyse the relative dynamics and address the relative GNC design for non-Keplerian orbits proximity operations. It is remarked that a high-fidelity dynamics modelling is fundamental to support the high-level design of 6DOF GNC strategies. The paper particularly stresses the beneficial effects of a coupled 6DOF analysis, to better leverage the natural dynamics to design effective and efficient approaching trajectories: the greater flexibility offered by the increased model complexity gets to a design that addresses GNC functional and performance requirements. On-board resource limitations and mission reliability is highlighted in the discussion. As an example, energy optimal rendezvous trajectories are discussed, considering the beneficial output of the coupled dynamics model, to trade off the proximity trajectory design and guidance strategy alternatives. Moreover, a relevant operative case study is presented to underline the fruitful effects of the coupled 6DOF and the relative dynamics approach here adopted for non-Keplerian orbit GNC design.

1. Introduction

Cislunar space is receiving a lot of attention from international space community thanks to its peculiar dynamical environment, which is able to boost and support the design of innovative space missions and infrastructures. In fact, within the proposed plans of future space exploration programmes, modular and extended space systems are intended to be available in cislunar non-Keplerian orbits to run robotic activities, in preparation of a safe and reliable operational outpost in the Moon vicinity for humans to come [1].

This fascinating exploration roadmap is based on the sustainability of the entire network of systems and operations to achieve the proposed ambitious goals, which would not be possible without a strong support of preliminary missions and new technologies development. In particular, as ISS operations teach, in-space outposts ask for complex logistic, which leans on rendezvous and docking/berthing capabilities between space segments and embrace different engineering disciplines. However, despite the available knowledge about proximity operations in Low-Earth Orbits (LEO), the development of this kind of missions asks for trajectory design and GNC techniques leveraging four-body problem dynamics and coupled orbit-attitude equations of motion. Literature studies deeply investigating 6DOF relative dynamics in non-Keplerian orbits are

Copyright © 2018 by Andrea Colagrossi. Published by the International Astronautical Federation with permission.

somewhat missing but, again, this area of investigation is now mandatory to support the design and implementation of cislunar infrastructures. Especially considering that the cislunar station will have to be assembled by means of several rendezvous and docking/berthing operations in non-Keplerian environments, being an Earth-Moon libration point orbit the ideal location for a space system of this kind [2].

In this direction, the paper discusses and justifies the 6DOF model, based on circular restricted and full ephemeris models, implemented to analyse the relative dynamics and address the relative GNC design for non-Keplerian orbits proximity operations. It is here anticipated that a high-fidelity dynamics modelling is fundamental to support the high-level design of 6DOF GNC strategies [3]. Similarly, the effects of rotational motion on rendezvous operations should not be neglected for large space structures, as already highlighted in previous works of the authors [4, 5].

The present research work is dedicated to propose effective and efficient strategies that could be exploited to sustainably assemble such a complex infrastructure in cislunar space. The paper starts introducing a 6DOF model for relative orbit-attitude dynamics in the Earth-Moon system. Then, 6DOF guidance and control functions are discussed, starting from energy optimal rendezvous trajectories and getting to GNC functional and performance requirements. On-board resource limitations and mission reliability is highlighted in the discussion. As example application, a relevant operative case study is presented to underline the fruitful effects of the coupled 6DOF and the relative dynamics approach here adopted for non-Keplerian orbit GNC design.

2. Orbit-attitude relative dynamics

The relative orbit-attitude dynamical model in cislunar space is based on the absolute dynamics within the restricted three-body problem modelling approach, which consider the motion of three masses m_1, m_2 and m, where $m \ll m_1, m_2$ and $m_2 < m_1$. m_1 and m_2 are referred to as primaries, and their orbits about their common centre of mass are assumed to be circular, in the circular restricted case, or according to numerical ephemerides, in the full ephemeris case. The differences between the two modelling cases will be discussed in the following. The body m does not affect the motion of the primaries.

The relative dynamics between two bodies of generic masses m_T and m_C is conveniently expressed in the inertial reference frame I, which is shown in figure 1, centred at the centre of mass of the primaries, O, and defined by the versors $\hat{X}$, $\hat{Y}$ and $\hat{Z}$. For analogy with classical works about three-body problem models, it could be convenient

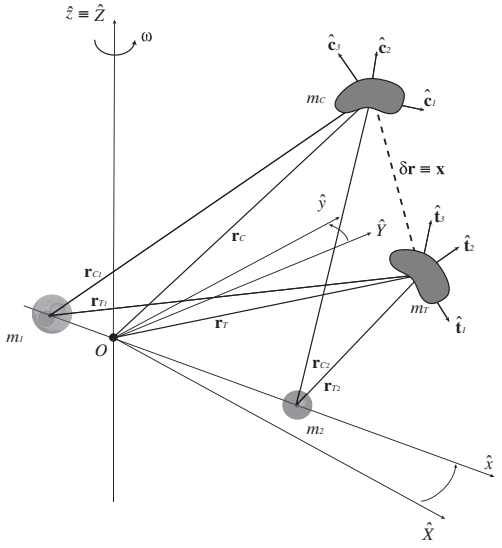

Fig. 1: Orbit-attitude relative dynamics.

to analyse certain results in a rotating synodic reference frame, S. This non-inertial frame is again centred in O, it is aligned to I at $t = 0$ and it is defined by the versors $\hat{x}$, $\hat{y}$ and $\hat{z}$: $\hat{x}$, is aligned with the vector from m_1 to m_2; $\hat{z}$, is in the direction of the angular velocity of S, $\boldsymbol{\omega} = \omega\hat{z}$; $\hat{y}$ completes the right-handed triad. Note that the hat symbol (i.e. $\hat{}$) represents versors. The system of the two primaries is defined by their mass parameter,

$$\mu = \frac{m_2}{m_1 + m_2},$$

by the magnitude of their mean angular velocity about $\hat{Z} \equiv \hat{z}$,

$$\omega = \sqrt{\frac{G(m_1 + m_2)}{r_{12}^3}},$$

and by their reciprocal distance r_{12}. The equations of motion can be normalised such that r_{12}, ω and the total mass of the system, $m_1 + m_2$, are unitary in non-dimensional units (symbol $[\mathrm{nd}]$).

The absolute orbit-attitude dynamics of the extended and three-dimensional bodies m_T, target, and m_C, chaser, has been modelled following the formulation described in the previous works of the authors [4]. It is here worth recalling that the absolute orbit-attitude dynamics is parametrized using the positions of the centres of mass of the bodies m_T and m_C, which are easily described by the position vectors $\mathbf{r}_T$ and $\mathbf{r}_C$, and the four-dimensional quaternion unit vectors, $\mathbf{q}_T$ and $\mathbf{q}_C$, also known as Euler parameters, which relates the body frames B_T and B_C with respect to the inertial frame I. The body-fixed frames B_T and B_C are centred at the centre of mass of the two

Copyright © 2018 by Andrea Colagrossi. Published by the International Astronautical Federation with permission.

bodies and are aligned with their principal inertia directions.

The relative orbit-attitude dynamics can be obtained from the absolute dynamics expressed in the frame I. The relative translational dynamics is immediately available from the definition of the relative position vector, $\mathbf{x}$:

$$\mathbf{x} \equiv \delta\mathbf{r} = \mathbf{r}_C - \mathbf{r}_T, \tag{1}$$

which, in the inertial reference frame, can be straightforwardly differentiated in time obtaining:

$$\ddot{\mathbf{x}} = \ddot{\mathbf{r}}_C - \ddot{\mathbf{r}}_T, \tag{2}$$

where $\ddot{\mathbf{r}}_C$ and $\ddot{\mathbf{r}}_T$ are the absolute acceleration vectors of chaser and target (i.e. the reference), available from the absolute dynamics equations. For readers' convenience, the absolute dynamics of the target in cislunar space is reported here in dimensional form:

$$\ddot{\mathbf{r}}_T = -\frac{\mu_E}{r_{T_E}^3}\mathbf{r}_{T_E} - \frac{\mu_M}{r_{T_M}^3}\mathbf{r}_{T_M} + \mathbf{a}_{T_S} + \mathbf{a}_{T_{SRP}}, \tag{3}$$

where the subscript 1 of the larger primary has been substituted with E (i.e. Earth) and the subscript 2 of the smaller primary with M (i.e. Moon). Note that symbols in bold font represent vectors, while the scalars are indicated in normal font. If the same symbol is used in bold and normal font, the former is the vector and the latter is its norm. $\mu_E = Gm_E$ and $\mu_M = Gm_M$ are the dimensional mass parameters. The terms $\mathbf{a}_{T_S}$ and $\mathbf{a}_{T_{SRP}}$ are the perturbing accelerations in cislunar space due to the gravitational presence of the Sun and due to the solar radiation pressure (SRP), which are the most relevant perturbations to be considered for the dynamics on Earth-Moon libration point orbits. These perturbations are modelled as typically done in astrodynamics literature [6, 7]. In particular, the Sun's gravity perturbations in Earth-Moon systems is expressed in the inertial frame as:

$$\mathbf{a}_{T_S} = -\mu_S\left(\frac{\mathbf{r}_{T_S}}{r_{T_S}^3} + \frac{\mathbf{r}_S}{r_S^3}\right), \tag{4}$$

where $\mu_S = Gm_S$, $\mathbf{r}_{T_S}$ is the position vector from the Sun to the Target in I and $\mathbf{r}_S$ is the position vector vector of the Sun with respect to O. In practice, the dynamics in cislunar space is set within a perturbed four-body problem model. When the circular restricted model is considered, the cislunar space is idealized and modelled as a classical bicircular problem, where the orbits of the Earth and the Moon about their common centre of mass are assumed to be circular, and the centre of mass of the Earth-Moon system is assumed to revolve around the centre of mass of the Earth-Moon-Sun system in a circular, coplanar motion. While, when the ephemeris model is considered, the position of Earth, Moon and Sun are available from numerical ephemerides contained in the SPICE Toolkit by NASA / JPL. In this last case, the cislunar space is accurately modelled neglecting just the minor perturbing effects. In fact, the relevant perturbations, which have a noticeable effect also in a short time scale, are included: orbital eccentricity and orbital inclination of the primaries, solar gravitation and solar radiation pressure.

The relative attitude dynamics requires more attention with respect to the translational one. In fact, it describes the rotational motion of the chaser relative to the target frame, or the other way around; in both cases, the relative attitude dynamics is expressed with respect to a non-inertial reference frame. First of all, a relative quaternion from B_T to B_C has to be defined as:

$$\delta\mathbf{q} = \mathbf{q}_C \times \mathbf{q}_T^{-1} = \begin{bmatrix} \boldsymbol{\chi}(\mathbf{q}_T)\mathbf{q}_C \\ \\ \mathbf{q}_T^{\mathrm{T}}\mathbf{q}_C \end{bmatrix}. \tag{5}$$

The matrix $\boldsymbol{\chi}(\mathbf{q}_T)$ is a 3×4 matrix defined as:

$$\boldsymbol{\chi}(\mathbf{q}_T) = \begin{bmatrix} q_{T_4}\mathbf{I}_{3\times 3} - [\mathbf{q}_{T_{123}}\times] & -\mathbf{q}_{T_{123}} \end{bmatrix}, \tag{6}$$

where $\mathbf{q}_{T_{123}} = [q_{T_1}, q_{T_2}, q_{T_3}]^{\mathrm{T}}$ is the column vector part and q_{T_4} is the scalar part of the target quaternion $\mathbf{q}_T$; $\mathbf{I}_{3\times 3}$ is the 3×3 identity matrix; $[\mathbf{q}_{T_{123}}\times]$ is the 3×3 skew-symmetric cross-product matrix, defined for a generic column vector, $\mathbf{u} = [u_1, u_2, u_3]^{\mathrm{T}}$, as:

$$[\mathbf{u}\times] = \begin{bmatrix} 0 & -u_3 & u_2 \\ u_3 & 0 & -u_1 \\ -u_2 & u_1 & 0 \end{bmatrix}. \tag{7}$$

The rotation matrix $\mathbf{R}$, which transform a vector from the target reference frame, B_T, to the chaser reference frame, B_C, can be expressed in terms of the relative quaternion $\delta\mathbf{q}$ as:

$$\mathbf{R}(\delta\mathbf{q}) = \begin{bmatrix} \delta\mathbf{q}_1^2 - \delta\mathbf{q}_2^2 - \delta\mathbf{q}_3^2 + \delta\mathbf{q}_4^2 & 2(\delta\mathbf{q}_1\delta\mathbf{q}_2 - \delta\mathbf{q}_3\delta\mathbf{q}_4) & 2(\delta\mathbf{q}_1\delta\mathbf{q}_3 + \delta\mathbf{q}_2\delta\mathbf{q}_4) \\ 2(\delta\mathbf{q}_1\delta\mathbf{q}_2 + \delta\mathbf{q}_3\delta\mathbf{q}_4) & -\delta\mathbf{q}_1^2 + \delta\mathbf{q}_2^2 - \delta\mathbf{q}_3^2 + \delta\mathbf{q}_4^2 & 2(\delta\mathbf{q}_2\delta\mathbf{q}_3 - \delta\mathbf{q}_1\delta\mathbf{q}_4) \\ 2(\delta\mathbf{q}_1\delta\mathbf{q}_3 - \delta\mathbf{q}_2\delta\mathbf{q}_4) & 2(\delta\mathbf{q}_2\delta\mathbf{q}_3 + \delta\mathbf{q}_1\delta\mathbf{q}_4) & -\delta\mathbf{q}_1^2 - \delta\mathbf{q}_2^2 + \delta\mathbf{q}_3^2 + \delta\mathbf{q}_4^2 \end{bmatrix}. \tag{8}$$

At this point, the relative angular velocity can be defined in I as:

$$\delta\boldsymbol{\omega}^I = \boldsymbol{\omega}_C^I - \boldsymbol{\omega}_T^I = \mathbf{A}_{I\,B_C}(\boldsymbol{\omega}_C^{B_C} - \mathbf{R}\,\boldsymbol{\omega}_T^{B_T}), \tag{9}$$

where $\mathbf{A}_{I\,B_C} = \mathbf{A}_{B_C I}^{\mathrm{T}}$ is the attitude matrix from the chaser frame B_C to the inertial frame I. Note that chaser and target angular velocities $\boldsymbol{\omega}_C^I$ and $\boldsymbol{\omega}_T^I$ are expressed in the inertial frame, while $\boldsymbol{\omega}_C^{B_C}$ and $\boldsymbol{\omega}_T^{B_T}$ are expressed in the body-fixed frames. Consequently, the relative angular velocity in B_C is simply:

$$\delta\boldsymbol{\omega}^{B_C} = \boldsymbol{\omega}_C^{B_C} - \mathbf{R}\,\boldsymbol{\omega}_T^{B_T}. \tag{10}$$

Copyright © 2018 by Andrea Colagrossi. Published by the International Astronautical Federation with permission.

Finally, it is possible to express the relative attitude dynamics of the chaser with respect to the target, in the body-fixed frame B_C, as:

$$\begin{aligned}\delta\dot{\boldsymbol{\omega}}^{B_C} = \mathbb{I}_C^{-1}\Big\{ &- [\delta\boldsymbol{\omega}^{B_C}\times]\mathbb{I}_C\delta\boldsymbol{\omega}^{B_C} - [\delta\boldsymbol{\omega}^{B_C}\times]\mathbb{I}_C\mathbf{R}\,\boldsymbol{\omega}_T^{B_T} \\ &+ \mathbb{I}_C[\delta\boldsymbol{\omega}^{B_C}\times]\mathbf{R}\,\boldsymbol{\omega}_T^{B_T} - [\mathbf{R}\,\boldsymbol{\omega}_T^{B_T}\times]\mathbb{I}_C\delta\boldsymbol{\omega}^{B_C} + \mathbf{n}_C \\ &- \mathbf{R}\Big[(\mathbf{R}^{\mathrm{T}}\mathbb{I}_C\mathbf{R} - \mathbb{I}_T)\mathbb{I}_T^{-1}(\mathbf{n}_T - [\boldsymbol{\omega}_T^{B_T}\times]\mathbb{I}_T\boldsymbol{\omega}_T^{B_T}) \\ &+ [\boldsymbol{\omega}_T^{B_T}\times](\mathbf{R}^{\mathrm{T}}\mathbb{I}_C\mathbf{R} - \mathbb{I}_T)\boldsymbol{\omega}_T^{B_T}\Big] - \mathbf{R}\,\mathbf{n}_T\Big\},\end{aligned} \tag{11}$$

where $\mathbb{I}_C$ and $\mathbb{I}_T$ are the inertia tensors of chaser and target in principal axes; $\mathbf{n}_C$ and $\mathbf{n}_T$ are the external torque vectors acting on the rigid bodies, respectively expressed in B_C and B_T [8]. In particular, the relevant external torques in cislunar space are: the gravity gradient torques of Earth and Moon, and the solar radiation pressure torque. Furthermore, in this work, also the gravity gradient torque of the Sun is taken into account as an external torque perturbation. These external contributions due to the environment have been modelled as done classically in literature [7].

From the relative attitude dynamics, which allows to compute the time evolution of the relative angular rates, the derivation of the attitude kinematics is immediate. In fact, the kinematic equation for the relative quaternion is:

$$\delta\dot{\mathbf{q}} = \frac{1}{2}\boldsymbol{\Omega}(\delta\boldsymbol{\omega}^{B_C})\delta\mathbf{q}, \tag{12}$$

where all the used variables are function of time and the matrix $\boldsymbol{\Omega}$ is a 4×4 skew-symmetric matrix defined as:

$$\boldsymbol{\Omega}(\boldsymbol{\omega}) = \begin{bmatrix} -[\boldsymbol{\omega}\times] & \boldsymbol{\omega} \\ -\boldsymbol{\omega}^{\mathrm{T}} & 0 \end{bmatrix}. \tag{13}$$

Knowing the relative orbit-attitude dynamics between target and chaser and assuming to have available the absolute orbit-attitude dynamics of the target (i.e. the reference), it is possible to have a complete understanding of both absolute and relative orbit-attitude dynamics involving two bodies in cislunar space.

For practical operational applications, both absolute (in reference [4]) and relative (in equations (2) and (11)) orbit-attitude dynamics can be propagated in-time with on-board software. In particular, the aforementioned dynamics is useful to increase the navigation accuracy with filters to better estimate the states available from sensors measurements. An example of navigation implementation is briefly discussed considering a chaser spacecraft equipped with sensors able to measure its relative state with respect to the target: a navigation filter, exploiting the developed relative orbit-attitude dynamics in non-Keplerian orbits, is applied to improve the accuracy of relative navigation, enabling the guidance functions to work in relative frames and compute the best trajectories for rendezvous and docking between the two spacecrafts. For what concern absolute navigation, it should be supported by ground-tracking (e.g. DSN), or, in order to have full on-board autonomy, alternative navigation techniques should be exploited (e.g. liaison navigation). However, when one of the two spacecrafts have accurate information about its absolute and relative states, the estimation of the absolute state of the other spacecraft is straightforward from the relations available.

Guidance and control functions, similarly to what has been discussed for the navigation functions, require the dynamics equations to be implemented. In this work, 6DOF relative GNC functions to perform rendezvous and docking in cislunar non-Keplerian orbits are discussed and, thus, equation (2) and equation (11) are of interest. These are exploited to compute the reference trajectories connecting chaser and target. Then, the control profile is needed in order to have the chaser moving on the desired rendezvous path. This work is not considering the control actuation and, hence, the discussion about 6DOF guidance and control is concluded when the nominal control acceleration profiles are available. In fact, the output of the control functions is a vector of linear accelerations in inertial frame I and a vector of angular accelerations in chaser body-fixed frame B_C. These control acceleration vectors, respectively $\mathbf{a}_C$ and $\boldsymbol{\alpha}_C$, are summed to the chaser absolute orbit-attitude dynamics. As a consequence, considering the formulation of equations (2) and (11), the controlled relative orbit-attitude dynamics equation are:

$$\ddot{\tilde{\mathbf{x}}} = \ddot{\mathbf{x}} + \mathbf{a}_C, \tag{14}$$

$$\delta\dot{\tilde{\boldsymbol{\omega}}}^{B_C} = \delta\dot{\boldsymbol{\omega}}^{B_C} + \boldsymbol{\alpha}_C. \tag{15}$$

2.1 Linearized relative dynamics

Guidance and control functions can be developed exploiting linear techniques and, in general, a linear formulation of the dynamics can be helpful. Therefore, to set up the framework for linear control design, a linearization of the relative dynamics about the target (i.e. reference) spacecraft state can be performed.

Translational relative dynamics can be linearized assuming the relative distance between chaser and target to be small compared to the distance between the target and the primaries: $\|\mathbf{x}\| \ll r_{T_E}$ and $\|\mathbf{x}\| \ll r_{T_M}$. In this way, a first order expansion of equation (2) is possible obtaining [9]:

$$\begin{bmatrix}\dot{\mathbf{x}} \\ \ddot{\mathbf{x}}\end{bmatrix} \approx \begin{bmatrix}\mathbf{0} & \mathbf{I}_{3\times 3} \\ \boldsymbol{\Xi}(t) & \mathbf{0}\end{bmatrix}\begin{bmatrix}\mathbf{x} \\ \dot{\mathbf{x}}\end{bmatrix}, \tag{16}$$

where $\boldsymbol{\Xi}(t)$ is a term dependent from the position of the target spacecraft. Hence, it is a term depending, as a function

Copyright © 2018 by Andrea Colagrossi. Published by the International Astronautical Federation with permission.

of time, on the known absolute orbital state of the target:

$$\begin{aligned}\boldsymbol{\Xi}(t) = &-\left(\frac{\mu_E}{r_{T_E}^3}+\frac{\mu_M}{r_{T_M}^3}\right)\mathbf{I}_{3\times3}+3\frac{\mu_E}{r_{T_E}^3}\left[\hat{r}_{T_E}\hat{r}_{T_E}^{\mathrm{T}}\right]\\&+3\frac{\mu_M}{r_{T_M}^3}\left[\hat{r}_{T_M}\hat{r}_{T_M}^{\mathrm{T}}\right],\end{aligned} \tag{17}$$

where the result of a first order expansion linearization is evident. Note that the relative perturbation terms due to the Sun's gravity and to the SRP are negligible in the linearization process, compared to the gravity field of the primaries. Even if their linearization is straightforward, these effects are treated as perturbations also in the linearized dynamic model, in order to avoid an eccessive computational burden. Equation (17) can be easily adapted to work with the circular restricted model or with the ephemeris model, since the differences stay only in the definition of the position vectors of the primaries: as sinusoidal circle functions or as numerical ephemerides. Analogously, the modification from dimensional units to normalized non-dimensional ones is immediate. As a last comment, equation (16) and equation (17) can be modified also to be formulated in synodic non-inertial reference frame: the matrix $\boldsymbol{\Xi}(t)$ requires only to be rotated from I to S, while the linear system in equation (16) has to take into account the non-inertial terms due to centrifugal and Coriolis effects. When the control is applied, considering also the relative perturbations, the linear dynamics equations become:

$$\begin{aligned}\begin{bmatrix}\dot{\tilde{\mathbf{x}}}\\ \ddot{\tilde{\mathbf{x}}}\end{bmatrix} \approx &\begin{bmatrix}\mathbf{0} & \mathbf{I}_{3\times3}\\ \boldsymbol{\Xi}(t) & \mathbf{0}\end{bmatrix}\begin{bmatrix}\tilde{\mathbf{x}}\\ \dot{\tilde{\mathbf{x}}}\end{bmatrix}+\begin{bmatrix}\mathbf{0}\\ \mathbf{I}_{3\times3}\end{bmatrix}\mathbf{a}_C\\&+\begin{bmatrix}\mathbf{0}\\ \mathbf{I}_{3\times3}\end{bmatrix}\left(\delta\mathbf{a}_S+\delta\mathbf{a}_{SRP}\right),\end{aligned} \tag{18}$$

where $\mathbf{a}_S$ and $\mathbf{a}_{SRP}$ are respectively the differential gravitational acceleration of the Sun and the differential acceleration due to solar pressure.

The relative attitude dynamics can be linearized as well. However, in this case, the assumptions is to have small attitude errors (i.e. $\delta\mathbf{q} \approx [0,0,0,1]^{\mathrm{T}}$) and small angular rates (i.e. $\boldsymbol{\omega}_C \approx \mathbf{0}$ and $\boldsymbol{\omega}_T \approx \mathbf{0}$). The first assumption allows to approximate the rotation matrix from B_T to B_C as $\mathbf{R} \approx \mathbf{I}_{3\times3}$, while the second assumption allows to neglect the cross angular rate terms as second order effects. Then, equation (15) becomes in the frame B_C:

$$\delta\dot{\tilde{\boldsymbol{\omega}}}^{B_C} \approx \mathbb{I}_C^{-1}\left\{\mathbf{n}_C-\mathbf{n}_T-\left[\mathbb{I}_C-\mathbb{I}_T\right]\mathbb{I}_T^{-1}\mathbf{n}_T\right\}+\boldsymbol{\alpha}_C, \tag{19}$$

which obviously reduces to

$$\delta\dot{\tilde{\boldsymbol{\omega}}}^{B_C} \approx \mathbb{I}_C^{-1}\mathbf{n}_C-\mathbb{I}_T^{-1}\mathbf{n}_T+\boldsymbol{\alpha}_C, \tag{20}$$

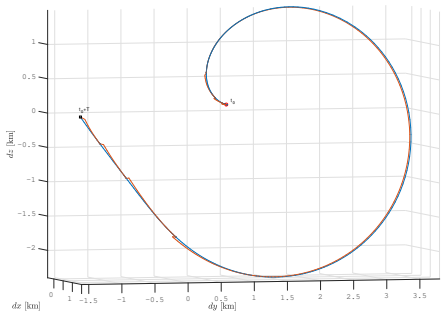

Fig. 2: Non-Keplerian orbit relative dynamics: non-linear (blue) and linearised with update time 1d (red). Example orbit L1 Halo with period T (t_0 at lunar pericentre).

where the external torque vectors are computed considering all the aforementioned external contributions within the assumptions of the linearized model. Accordingly, the linearized attitude kinematics becomes:

$$\delta\dot{\mathbf{q}} \approx \frac{1}{2}\begin{bmatrix}\delta\boldsymbol{\omega}^{B_C\tilde{\cong}B_T}\\ 0\end{bmatrix}. \tag{21}$$

Note that with these assumptions the target and chaser body frames, B_C and B_T, are approximately equivalent.

2.1.1 Validity of linearized relative dynamics

The assumptions behind the linearized equations of motions are very simple and it is easy to check if they are respected. However, those associated with linearized relative attitude dynamics are very strict and it is very difficult that they are respected during operational scenarios or, even during simple simulated settings. They are useful for certain applications like, for instance, stability studies and linear control analyses. Anyhow, they will not be employed in the following applications discussed in this paper. On the contrary, linearized relative translational dynamics is valid whenever the relative distance between chaser and target is smaller when compared to the distance between target and primaries. This condition is likely to be satisfied at all times during typical rendezvous operations. In fact, previous studies of the authors show that when the relative distance, $\|\mathbf{x}\|$, is below $10^2 - 10^3\,\mathrm{km}$, depending on the target orbital state, the linearized equations (16) and (18) are valid [3]. Therefore, the linearized dynamics is valid to approximate relative trajectories during rendezvous phases and it can be used to propagate the relative dynamics updating the relative state vector with a certain frequency.

In figure 2 the relative dynamics simulated for an orbital period, T, along an example L1 Halo orbit is shown; the simulation is started at the pericentre of the orbit and the relative state is updated every day. The ephemeris model

Copyright © 2018 by Andrea Colagrossi. Published by the International Astronautical Federation with permission.

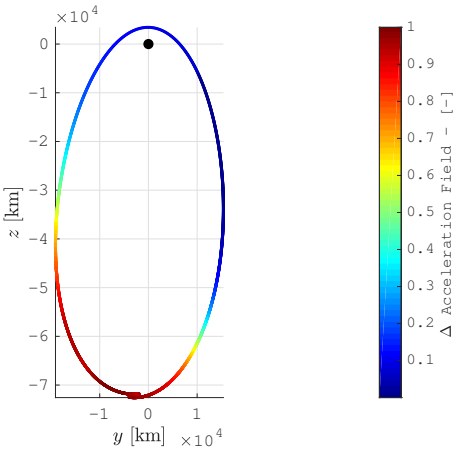

Fig. 3: Circular restricted and ephemeris models comparison in relative dynamics modelling on NRHOs (results are normalized with respect to the maximum difference in the relative acceleration).

with perturbations has been used. From this example, it is evident that the propagation error has an evolution trend that is dependent on the point along the orbit: at the apocentre (i.e. $r_{T_M} \sim 10^4\,\mathrm{km}$) the linearised model gives acceptable results for a longer time with respect to the pericentre (i.e. $r_{T_M} \sim 10^3\,\mathrm{km}$). At the apocentre, the assumption to have the relative distance much smaller than the distance of the target from the primaries is definitely valid, with greater tolerance with respect to the pericentre. The acceptable duration of propagation time depends on GNC requirements: in the discussed example, the update time of the linearised model to maintain the error with respect to the full dynamics below $10\,\mathrm{cm}$ is of $\sim 3\,\mathrm{h}$ at apocentre and $\sim 40\,\mathrm{s}$ at the pericentre of the reference orbit.

2.2 Circular restricted and ephemeris models comparison

Circular restricted model is valuable for preliminary analysis of non-Keplerian orbits. Nevertheless, the very peculiar regime of the Earth-Moon system is strongly dependent from the true motion of Earth and Moon, since their orbital eccentricity is not negligible in dictating the force field that maintains the periodicity of non-Keplerian orbits. In particular, for what concern relative dynamics, even in the short period, the ephemeris four-body model is the model to correctly represent the peculiar regime of relative motion in cislunar space.

For example, when a Near Rectilinear Halo Orbits (NRHO) is considered, in figure 3, the error between circular restricted model and ephemeris model is particularly relevant whenever the distance of the target from the Moon is above a certain value: at the apocentre of the example orbit, the error in the relative acceleration is 30% in magnitude and $20°$ in direction. On the contrary, at the pericentre of the orbit there is a little deviation, because the close vicinity to the Moon makes all the effects not considered in the circular model of minor importance with respect to the gravitational pull of the Moon, which is well represented in both models.

A Near Rectilinear Halo Orbit has been chosen to perform this comparison because it spans a wide range of distances from the Moon, it is non-planar and its is of great interest for practical applications. In fact, NRHOs have been often proposed as staging orbits in cislunar space by international space agencies, because many of their properties are suitable to host a possible cislunar space station [2]. This family of non-Keplerian orbits is in the focus of this research work because of their applicative relevance. Moreover, they allows the highlight several peculiarities of dynamics in the Earth-Moon system, and the outcomes discussed in this study can be easily extended to the other families of cislunar orbits.

The circular restricted model do not provide generally valid approximations of the relative dynamics in the Earth-Moon system and its validity should be assessed for each particular case that is analysed. Therefore, it is not considered in the followings. The model that should be used to investigate the relative dynamics in cislunar space is the ephemeris four-body model with perturbations.

3. Relative orbit-attitude guidance and control design

Relative orbit-attitude guidance and control (GC) design is based on full non-linear relative dynamics equations (14) and (15). However, a first insight about the possibilities to control the relative dynamics between two spacecrafts in non-Keplerian orbits is available exploiting the linearized translational dynamics together with the full rotational dynamics; they are implemented with the ephemeris four-body model with perturbations.

3.1 Energy optimal 6DOF guidance and control

The requirements for the sustainability of the entire network of systems and operations to realize the forthcoming space programmes in cislunar space and beyond impose a certain attention while analysing and designing the elements that will compose the whole mission scenario. For this reason, this research work starts investigating the rendezvous and docking operations in cislunar space under the framework of energy optimal applications. Obviously, other alternatives are equally valid, like, for example, time optimal or sub-optimal robust solutions. Analogously, different optimality criterions can be foreseen during the design of guidance and control functions or, additional

Copyright © 2018 by Andrea Colagrossi. Published by the International Astronautical Federation with permission.

operational and functional requirements can force the design out of the classical optimal control concepts. An hint about a possible operational implementation of rendezvous functions will be discussed later in the paper.

Anyhow, an energy optimal control design is here discussed. In fact, the optimal rendezvous problem can be solved because the absolute dynamics of the chaser is controlled by a control variable,

$$\mathbf{u} = \left[\frac{a_{C_x}}{a_{C_{x}max}}, \frac{a_{C_y}}{a_{C_{y}max}}, \frac{a_{C_z}}{a_{C_{z}max}}, \frac{\alpha_{C_1}}{\alpha_{C_{1}max}}, \frac{\alpha_{C_2}}{\alpha_{C_{2}max}}, \frac{\alpha_{C_3}}{\alpha_{C_{3}max}}\right]^{\mathrm{T}}, \tag{22}$$

which is representative of the 6DOF normalized control accelerations, respectively defined in the inertial frame and in the chaser body-fixed frame. Both are expressed in cartesian coordinates, as the relative equations of motion in equations (15) and (18). For sake of simplicity, it is assumed that $a_{C_i max} = 1\,\mathrm{ms}^{-2}$ and $\alpha_{C_j max} = 1\,\mathrm{rads}^{-2}$, for $i = x, y, z$ and $j = 1, 2, 3$. All six controls are bounded: $-\mathbf{1} \leq \mathbf{u} \leq \mathbf{1}$.

The analysis starts solving the optimal rendezvous problem with a constrained indirect optimisation.

3.1.1 Objective function

The objective function is written according to Lagrange's problem formulation:

$$J = \int_{t_0}^{t_f} \mathcal{L}\, dt, \tag{23}$$

where t_0 and t_f are respectively the initial and final time of the rendezvous phase, while $\mathcal{L}$ is the Lagrangian of the problem, whose analytical expression depends on the particular optimisation problem to be solved. Again, in this work the minimum energy problem (i.e. minimum quadratic control) is addressed. Hence, the Lagrangian function is:

$$\mathcal{L} = \frac{1}{2}\left(\mathbf{u}\cdot\mathbf{u}\right). \tag{24}$$

3.1.2 Boundary conditions

The boundary conditions of the problem are defined in a way that the overall optimal rendezvous problem would be as simple as possible. However, these boundary conditions are effective to have a well posed problem. The target and chaser initial states and, thus, the relative state at $t = t_0$ are fully assigned:

$$\mathbf{x}(t_0) = [x_0, y_0, z_0]^{\mathrm{T}}, \tag{25}$$

$$\dot{\mathbf{x}}(t_0) = [v_{x_0}, v_{y_0}, v_{z_0}]^{\mathrm{T}}, \tag{26}$$

$$\delta\mathbf{q}(t_0) = [\delta q_{1_0}, \delta q_{2_0}, \delta q_{3_0}, \delta q_{4_0}]^{\mathrm{T}}, \tag{27}$$

$$\delta\boldsymbol{\omega}^{B_C}(t_0) = \left[\delta\omega_{1_0}^{B_C}, \delta\omega_{2_0}^{B_C}, \delta\omega_{3_0}^{B_C}\right]^{\mathrm{T}}. \tag{28}$$

At final time $t = t_f$ the rendezvous has to be completed. The relative state is, accordingly:

$$\mathbf{x}(t_f) = [0, 0, 0]^{\mathrm{T}}, \tag{29}$$

$$\dot{\mathbf{x}}(t_f) = [0, 0, 0]^{\mathrm{T}}, \tag{30}$$

$$\delta\mathbf{q}(t_f) = [0, 0, 0, 1]^{\mathrm{T}}, \tag{31}$$

$$\delta\boldsymbol{\omega}^{B_C}(t_f) = [0, 0, 0]^{\mathrm{T}}. \tag{32}$$

All the boundary conditions are direct for a total of 26 direct explicit boundary conditions. In this section, the state variables are always related with a control action and, to simplify the notation, the tilde symbol over the variables (i.e. ˜) is discarded.

Further investigations about attitude rendezvous boundary conditions are discussed during the operative case study; in particular, the possibility to have different attitude boundary conditions is addressed. However, as will be discussed next, relative attitude states equal to zero at final time is of importance also for practical applications that take into account natural dynamics. Finally, it should be noted that, in real cases, the position vector of the docking points with respect to the centres of mass is not zero. In these situations, docking-enabling conditions should be defined taking into account the coupled orbit-attitude relative dynamics: the boundary conditions at $t = t_f$ are coupled with all the six degrees of freedom.

3.1.3 Hamiltonian function

The general formulation for the Hamiltonian of the system with the state vector $\mathbf{v} = [\mathbf{x}^{\mathrm{T}}\ \dot{\mathbf{x}}^{\mathrm{T}}\ \delta\mathbf{q}^{\mathrm{T}}\ \delta\boldsymbol{\omega}^{B_C\,\mathrm{T}}]^{\mathrm{T}}$, the control vector $\mathbf{u}$, the costate vector $\boldsymbol{\lambda} = [\boldsymbol{\lambda}_{\mathbf{x}}^{\mathrm{T}}\ \boldsymbol{\lambda}_{\dot{\mathbf{x}}}^{\mathrm{T}}\ \boldsymbol{\lambda}_{\delta\mathbf{q}}^{\mathrm{T}}\ \boldsymbol{\lambda}_{\delta\boldsymbol{\omega}^{B_C}}^{\mathrm{T}}]^{\mathrm{T}}$ and the Lagrangian $\mathcal{L}$, associated with the objective function in equation (23), is:

$$\begin{aligned}
H(\mathbf{v},\mathbf{u},\boldsymbol{\lambda}) &= \mathcal{L} + \boldsymbol{\lambda}\cdot[\dot{\mathbf{x}}^{\mathrm{T}}\ \ddot{\mathbf{x}}^{\mathrm{T}}\ \delta\dot{\mathbf{q}}^{\mathrm{T}}\ \delta\dot{\boldsymbol{\omega}}^{B_C\,\mathrm{T}}]^{\mathrm{T}} \\
&= \mathcal{L} + \boldsymbol{\lambda}_{\mathbf{x}}^{\mathrm{T}}\dot{\mathbf{x}} + \boldsymbol{\lambda}_{\dot{\mathbf{x}}}^{\mathrm{T}}\Big(\boldsymbol{\Xi}(t)\mathbf{x} + \delta\mathbf{a}_S + \delta\mathbf{a}_{SRP} + \mathbf{a}_C\Big) \\
&+ \boldsymbol{\lambda}_{\delta\mathbf{q}}^{\mathrm{T}}\Big(\frac{1}{2}\boldsymbol{\Omega}(\delta\boldsymbol{\omega}^{B_C})\delta\mathbf{q}\Big) \\
&+ \boldsymbol{\lambda}_{\delta\boldsymbol{\omega}^{B_C}}^{\mathrm{T}}\Bigg(\mathbb{I}_C^{-1}\Big\{-[\delta\boldsymbol{\omega}^{B_C}\times]\mathbb{I}_C\delta\boldsymbol{\omega}^{B_C} \\
&- [\delta\boldsymbol{\omega}^{B_C}\times]\mathbb{I}_C\mathbf{R}\,\boldsymbol{\omega}_T^{B_T} + \mathbb{I}_C[\delta\boldsymbol{\omega}^{B_C}\times]\mathbf{R}\,\boldsymbol{\omega}_T^{B_T} \\
&- [\mathbf{R}\,\boldsymbol{\omega}_T^{B_T}\times]\mathbb{I}_C\delta\boldsymbol{\omega}^{B_C} + \mathbf{n}_C \\
&- \mathbf{R}\Big[(\mathbf{R}^{\mathrm{T}}\mathbb{I}_C\mathbf{R} - \mathbb{I}_T)\mathbb{I}_T^{-1}(\mathbf{n}_T - [\boldsymbol{\omega}_T^{B_T}\times]\mathbb{I}_T\boldsymbol{\omega}_T^{B_T}) \\
&+ [\boldsymbol{\omega}_T^{B_T}\times](\mathbf{R}^{\mathrm{T}}\mathbb{I}_C\mathbf{R} - \mathbb{I}_T)\boldsymbol{\omega}_T^{B_T}\Big] \\
&- \mathbf{R}\,\mathbf{n}_T\Big\} + \boldsymbol{\alpha}_C\Bigg).
\end{aligned} \tag{33}$$

Copyright © 2018 by Andrea Colagrossi. Published by the International Astronautical Federation with permission.

The part of the Hamiltonian that depends on the controls, $\mathbf{u}$, is:

$$H^*(\mathbf{u}, \boldsymbol{\lambda}) = \frac{1}{2}(\mathbf{u} \cdot \mathbf{u}) + \boldsymbol{\lambda}_{\dot{\mathbf{x}}}^{\mathrm{T}} \mathbf{a}_C + \boldsymbol{\lambda}_{\delta\boldsymbol{\omega}^{B_C}}^{\mathrm{T}} \boldsymbol{\alpha}_C, \quad (34)$$

where the physical dimensions are uniformed because of the costate dimensions definition (i.e. normalized non-dimensional Hamiltonian function, according to the control variable expression in equation (22)).

3.1.4 Optimal control problem

Optimal control problem solved through indirect methods, which are based on the calculus of variation, requires a strong analytical effort to derive all the necessary quantities for the solution of the problem itself.

The costate dynamics adjoint equations are obtained as:

$$\dot{\boldsymbol{\lambda}} = -\left(\frac{\partial H}{\partial \mathbf{v}}\right). \quad (35)$$

It can be noted how the costates dynamics is intimately related to the state dynamics and the results are obviously dependent from the formulation of the relative dynamics itself. For example, the dynamics of the costates associated with translational dynamics result to be linear because of the linear dependance from $\mathbf{x}$ and $\dot{\mathbf{x}}$ in the relative dynamics, equation (18). Thus, when the Hamiltonian is differentiated with respect to these state variables the dependance from the state itself is lost: the translational costates evolution is just a function of the translational costates themselves and of the target (i.e. reference) trajectory in time. This is not the case for the costates related with the rotational motion, which is formulated through non-linear equations. Here, the attitude states are directly influencing the rotational costates dynamics that, in general, is non-linear.

For what concern the control equations for the minimum energy problem (in equation (24)), the 6 controls enters the Hamiltonian quadratically and, therefore, the optimal control results to be linearly dependent from the costates. In particular, control equations can be derived from:

$$\left(\frac{\partial H}{\partial \mathbf{u}}\right) = \left(\frac{\partial H^*}{\partial \mathbf{u}}\right) = 0. \quad (36)$$

The result of the previous equations states that the control actions have a magnitude defined by the magnitude of the costates associated with the velocities and a direction parallel and opposite to it:

$$\mathbf{u} = [-\boldsymbol{\lambda}_{\dot{\mathbf{x}}}^{\mathrm{T}}, -\boldsymbol{\lambda}_{\delta\boldsymbol{\omega}^{B_C}}^{\mathrm{T}}] \text{ with } \|\mathbf{u}\| < u_{max}. \quad (37)$$

3.1.5 Optimality and Transversality Conditions

The solution of the optimal control problem requires additional constraints with respect to the boundary conditions on the state at $t = t_0$ and $t = t_f$. In fact, the number of variables involved is definitely increased.

Optimality conditions, given the complete set of 26 direct boundary conditions on the initial and finale states, results in trivial conditions. In fact, the terms $d\mathbf{x}(t_0)$ and $d\mathbf{x}(t_f)$ are zero, and the costates at initial time, $\boldsymbol{\lambda}(t_0)$, and at final time, $\boldsymbol{\lambda}(t_f)$, are free.

Transversality conditions, which are additional necessary conditions for optimality, are dependent only from the Hamiltonian, given again the complete set of 26 direct boundary conditions on the initial and final states. The initial Hamiltonian, $H(t_0)$, is free because t_0 is assigned. On the contrary, the final time t_f is not assigned, because it is unknown: in the considered rendezvous problem, the time-of-flight (TOF) is free. Hence, the transversality condition at the final time states $H(t_f)dt_f = 0$, constraining the Hamiltonian evaluated at t_f as:

$$H(t_f) = 0. \quad (38)$$

3.1.6 Numerical implementation

The numerical implementation of the optimal control problem is based on a Matlab code. A finite difference code based on collocation (three-stage Lobatto IIIa formula) integrated into Matlab is applied to solve the two-point boundary value problem (TPBVP) associated with the indirect methods for the optimal control.

The initial guess for the costates is chosen as a set of zeros in the minimum energy problem. The differential equations are integrated with a variable-step, variable-order (VSVO) Adams-Bashforth-Moulton solver.

To solve the optimal control problem with a free final time exploiting this numerical implementation, the final time must be included as an unknown parameter. This is accomplished by non-dimensionalizing the time as:

$$\tau = \frac{t}{t_f} \rightarrow \frac{\mathrm{d}}{\mathrm{d}\tau} = t_f \frac{\mathrm{d}}{\mathrm{d}t} \text{ with } \tau \in [0, 1]. \quad (39)$$

3.1.7 Example optimal control results

An example result about the optimal control 6DOF rendezvous is shown, to prove the capabilities of the developed method, in figures 4 and 5. Initial relative states are random, while the target is moving with the periodic orbit-attitude dynamics close the apocentre of a L1 NRHO orbit [4, 10]. The control output is reported in terms of forces and torques in figures 4c and 5c. The chaser has a mass $m_C \sim 10^3\,\mathrm{kg}$ and the inertia moments $\mathbb{I}_C \sim 10^4\,\mathrm{kgm}^2$. The control action, as expected, is larger only at departure point and arrival point: consequently, the required control energy is minimized. Note that, the control force is linear in time, while the control torque has an evident non-linear trend. The relative velocities in figures 4b and 5b are extremely small and to minimize the control effort the required time is long.

Copyright © 2018 by Andrea Colagrossi. Published by the International Astronautical Federation with permission.

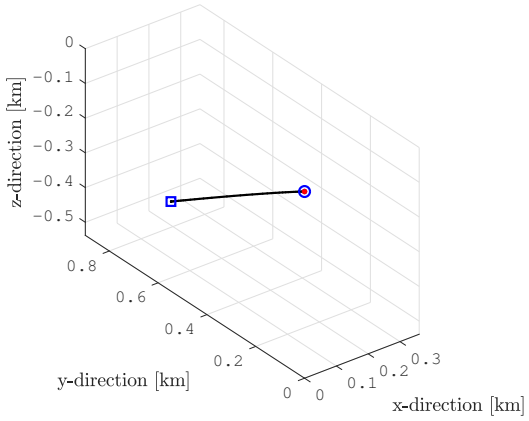

(a) Relative trajectory (t_0 blue square, t_f blue circle).

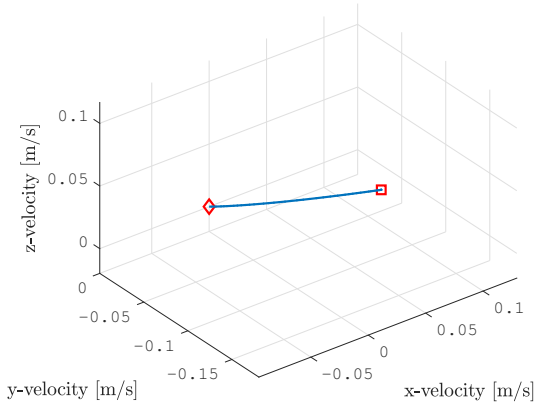

(b) Relative velocity (t_0 red square, t_f red diamond).

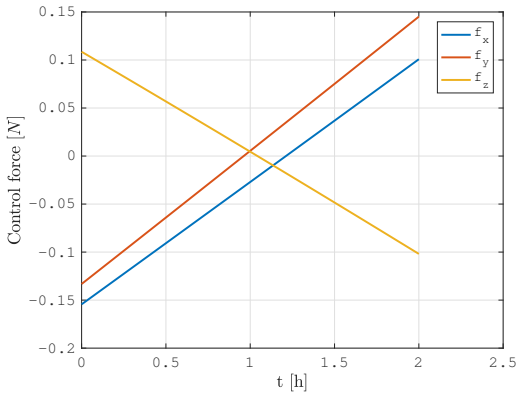

(c) Control force. Chaser mass: $m_C \sim 10^3$ kg.

Fig. 4: Optimal control for 6DOF rendezvous: translational dynamics. TOF: $t_f = 2$ h. Initial relative states random.

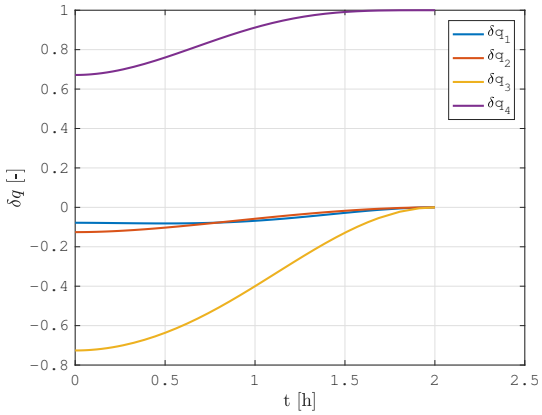

(a) Relative quaternion.

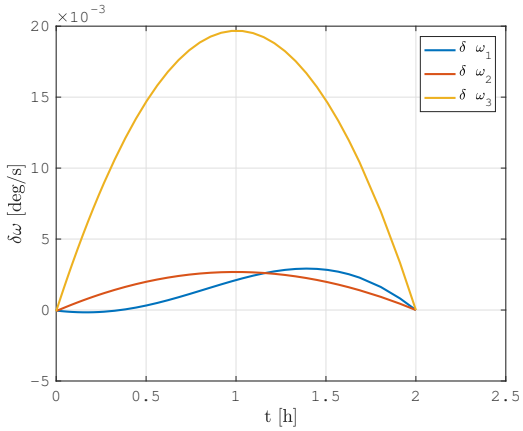

(b) Relative angular velocity.

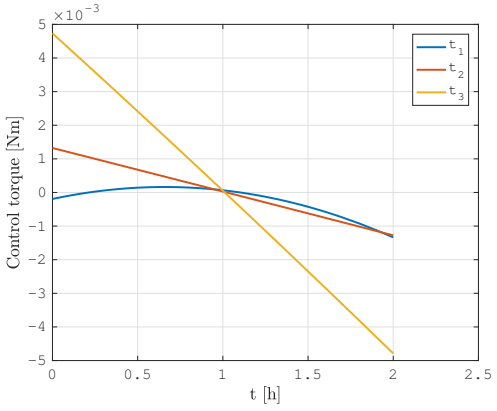

(c) Control torque. Chaser inertia moments: $\mathbb{I}_C \sim 10^4$ kgm^2.

Fig. 5: Optimal control for 6DOF rendezvous: rotational dynamics. TOF: $t_f = 2$ h. Initial relative states random.

Copyright © 2018 by Andrea Colagrossi. Published by the International Astronautical Federation with permission.

The algorithm provides an optimal solutions of the problem, in terms of quadratic control effort, but it requires quite few analyses to select a good initial guess for the costates. In particular, this is necessary when the initial relative states are complex and the rendezvous trajectories are not straightforward. For simple rendezvous scenarios, as the one discussed in this section, a vectors of zeros works decently as initial guess for the costates.

3.2 Direct transcription of the rendezvous problem

Indirect methods rely on analytical relations and the conditions for optimality require the solution of a two-point boundary value problem. It is well known that indirect methods ensures rapid convergence of good starting guesses, but most of the difficulties are related to the high sensitivity to the initial costates. As previously noted, it is difficult and time consuming to select a good initial guess for the costates. Their lack of physical meaning makes also difficult to have insights about their behaviour, in order to understand which could be a possibile good initial guess from previously converged solutions. In particular, these difficulties arise when a solution in the full non-linear relative dynamics is sought.

For the applications investigated in this research work, a more robust method is needed: the optimal rendezvous problem is now solved with direct methods, parametrizing only the control variable and converting the optimal control problem into a non-linear programming (NLP) problem, with a direct transcription process. Direct methods requires often a large computation effort but they are usually robust and can accommodate path constraints.

The solution of a generic non-linear programming problem is a vector of n variables, $\mathbf{p}$, that minimizes a scalar objective function:

$$\min_{\mathbf{p}} F(\mathbf{p}), \tag{40}$$

subject to m equality or inequality constraints:

$$\mathbf{b}_l \leq \mathbf{c}(\mathbf{p}) \leq \mathbf{b}_u, \tag{41}$$

and bounds:

$$\mathbf{p}_l \leq \mathbf{p} \leq \mathbf{p}_u. \tag{42}$$

The equality constraints are obtained imposing $\mathbf{b}_l = \mathbf{b}_u$.

With direct methods, the differential dynamic constraints of the indirect optimal rendezvous problem are converted into a set of algebraic constraints.

3.2.1 Control parametrization

From the results available, which have been discussed in section 3.1, it is possible to select a parametrization for the control variable that is as close as possible from the available solution of the optimal rendezvous problem solved with indirect methods: linear control for the translational dynamics and polynomial control for the rotational dynamics.

However, now the 6DOF dynamic is fully non-linear and the solution for a general rendezvous problem has to be found. For this reason, more flexibility in the control variable parametrization is sought, without discretizing the rendezvous path in multiple arches connected by patch points, and without increasing too much the complexity of the control actions. Different parametrization possibilities have been analysed, but the best results have been obtained with polynomials and Fourier series representations. Fourier series are known to have good convergence properties and polynomials are simple and effective, especially considering the optimal control available from indirect optimization methods.

Practically, polynomials up to the third degree and Fourier series up to the fourth order are used. The limitations in the degree of the expansions are imposed to limit the number of involved parameters, thus, the dimension n of the NLP problem. These possible parametrization options proved to have acceptable convergence properties and allowed to find a solution for the general rendezvous problem. As example, the control parametrization with a second degree polynomial for the translational control and a with a fourth order Fourier series for the rotation control results in:

$$\mathbf{a}_C(t) = \mathbf{a}_0 + \mathbf{a}_1 \left(\frac{t}{t_{ref}}\right) + \mathbf{a}_2 \left(\frac{t}{t_{ref}}\right)^2, \tag{43}$$

$$\boldsymbol{\alpha}_C(t) = \frac{\boldsymbol{\alpha}_0}{2} + \sum_{k=1}^{4} \left[\boldsymbol{\alpha}_k \cos\left(k\boldsymbol{\tau}\frac{t}{t_{ref}}\right) + \boldsymbol{\beta}_k \sin\left(k\boldsymbol{\tau}\frac{t}{t_{ref}}\right) \right], \tag{44}$$

where $\mathbf{a}_i$, $\boldsymbol{\alpha}_i$, $\boldsymbol{\beta}_i$ and $\boldsymbol{\tau}$ are 3×1 parameters vectors defined, respectively, in the reference frames I and B_C. The physical dimensions of these parameters are defined according to the physical quantity they are parametrizing. These parameters compose the vector of unknown variables, $\mathbf{p} = \left[\mathbf{a}_i^{\mathrm{T}}, \boldsymbol{\alpha}_i^{\mathrm{T}}, \boldsymbol{\beta}_i^{\mathrm{T}}, \boldsymbol{\tau}^{\mathrm{T}}, t_f\right]^{\mathrm{T}}$, to be found solving the problem in equation (40). The reference time, t_{ref}, is needed to non-dimensionalize the time, t, in the parametrized control functions. The choice of a reference time equal to the rendezvous TOF has proved to work well.

The dimension n of the NLP associated to the energy optimal rendezvous problem depends from the selected parametrization of the control functions $\mathbf{a}_C(t)$ and $\boldsymbol{\alpha}_C(t)$. For example, in the case the selected parametrization is the one shown in equations (43) and (44), the vector $\mathbf{p}$ has a dimensions of 40: 9 are the parameters for $\mathbf{a}_C(t)$,

Copyright © 2018 by Andrea Colagrossi. Published by the International Astronautical Federation with permission.

30 are the parameters for $\boldsymbol{\alpha}_C(t)$ and 1 parameter is the rendezvous TOF: t_f. Again, note that the selection of $t_{ref} = t_f$ allows a smooth convergence of the control parametrization.

The constraints in equation (41) are obtained from numerical integration of the controlled rendezvous dynamics. In fact, given a generic vector $\bar{\mathbf{p}}$ the relative dynamics has a certain evolution; the relative states at the end of the particular rendezvous simulations have to satisfy the imposed boundary conditions at the final time in equations (29) to (32). For example, the boundary conditions on the relative position is enforced as:

$$\mathbf{x}|_{\bar{\mathbf{p}}}(\bar{t}_f) = [0, 0, 0]^{\mathrm{T}}, \tag{45}$$

where $\mathbf{x}|_{\bar{\mathbf{p}}}$ is the relative position state, output of the relative dynamics, in equation (14), with $\mathbf{a}_c|_{\bar{\mathbf{p}}}(t)$.

The bounds in equation (42) are imposed to respect the physical meanings of the parameters. For example, the bounds on t_f are:

$$0 \leq t_f \leq t_{f_{Max}}, \tag{46}$$

where $t_{f_{Max}}$ is the imposed time limit to complete the rendezvous. The bounds on the remaining parameters are selected in order to have $\|\mathbf{u}(t)\| < u_{max}$ for any $t_0 \leq t \leq t_f$.

The optimality in terms of minimum energy control (i.e. minimum quadratic) is achieved defining the scalar objective function in equation (40) as:

$$F(\bar{\mathbf{p}}) = \frac{1}{2} \int_{\bar{t}} \mathbf{u}|^{\mathrm{T}}_{\bar{\mathbf{p}}}(t)\ \mathbf{u}|_{\bar{\mathbf{p}}}(t)\, dt, \tag{47}$$

where $\bar{t}$ is the rendezvous time from t_0 to $\bar{t}_f$. The integral is computed numerically, from the control parametrization functions, knowing just the value of $\bar{\mathbf{p}}$. Therefore, the computation of the objective function is extremely fast. Equation (47) is the analogous, in the direct transcription of the optimal rendezvous problem, to equation (23), in the Lagrange's formulation of the optimal control problem.

3.2.2 Numerical implementation

The numerical implementation of the optimal control problem is based on a Matlab code. A constrained minimization algorithm that is integrated into Matlab is applied to solve the non-linear programming problem associated with the direct transcription of the optimal control. The algorithm exploits sequential quadratic programming (SQP) method to solve the rendezvous.

The initial guess for the parameters in the vector $\mathbf{p}$ is random, normally distributed within the bounds for the parameters. The initial guess for the rendezvous TOF is given according to the desired order of magnitude for t_f. The differential equations are integrated with a VSVO Adams-Bashforth-Moulton solver. The numerical evaluation of the objective function is performed with a trapezoidal numerical integration algorithm over a vector equally spaced in time from t_0 to t_f.

3.2.3 Example direct transcription results

An example result about the direct transcription control for 6DOF rendezvous is shown, to prove the capabilities of the developed method, in figures 6 and 7. Initial relative states are random, while the target is moving with the periodic orbit-attitude dynamics close the apocentre of a L1 NRHO orbit [4, 10]. The control output is reported in terms of forces and torques in figures 4c and 5c. The chaser inertia properties are the same of the previous example about optimal control. The control has been parametrized according to the example functions in equations (43) and (44). Again, the control action is larger at departure point and arrival point: consequently, the required control energy is minimized. Note that, the control force is almost linear in time, despite it has been parametrized through a quadratic function. In fact, in this case, the minimization algorithm reduces almost to zero the parameters $\mathbf{a}_2$, related with the second order term. This result is expected and prove the correct convergence to a solution close to the one that could have been available with the indirect optimal control method. Note that since the close relative distance of the chaser with respect to the target, the differences between linear and non-linear translational dynamics are limited.

The control torque is evidently exploiting the parametrization capabilities of the Fourier series. The attitude control torque has a regular behaviour, which is again almost linear to minimize the quadratic objective function. The Fourier series parametrization of the attitude control requires little more time to converge, but it is usually providing better results in terms of control cost. In fact, from the analyses carried out, a simpler polynomial parametrization for $\boldsymbol{\alpha}_C$ is quick to converge but provides worse solution in terms of cost. Typically, the difference resulted to be in the order of $10 - 20\%$. For what concern, the translational control parametrization, $\mathbf{a}_C$, there have been no advantages in using the Fourier parametrization. Thus, the quadratic function discussed in this paper proved its effectiveness and efficiency for the direct transcription of the optimal translation rendezvous problem in cislunar space.

The algorithm is highly robust and converges quite easily, except for situations where the requested TOF for the rendezvous is out of the control capabilities (e.g. too short) or extremely long. In fact, the NLP solver has the authority to change t_f but, in general, the solution stays in proximity of the given initial guess for the TOF. The reason can be sought in the fact that changing the TOF creates a

Copyright © 2018 by Andrea Colagrossi. Published by the International Astronautical Federation with permission.

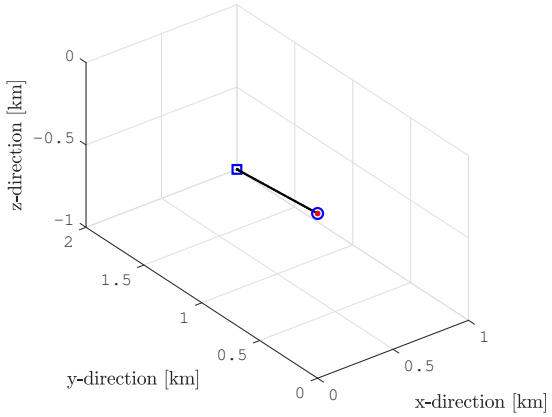

(a) Relative trajectory (t_0 blue square, t_f blue circle).

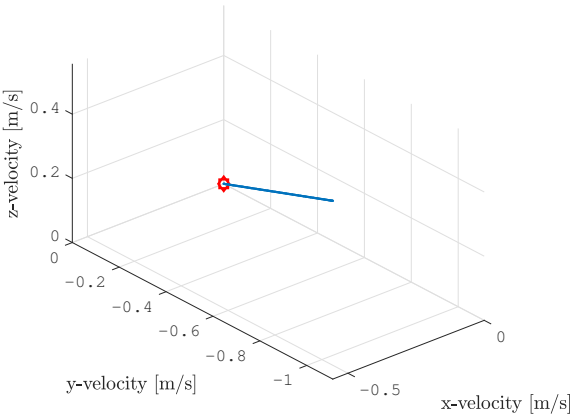

(b) Relative velocity (t_0 red square, t_f red diamond).

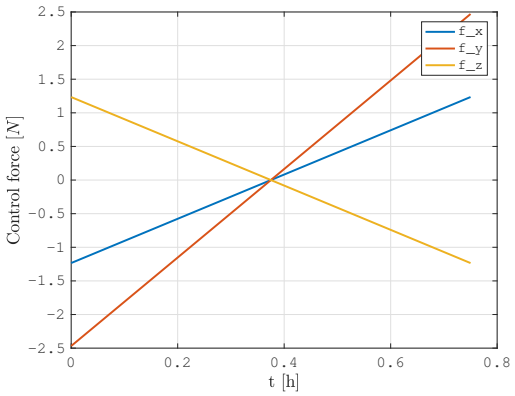

(c) Control force. Chaser mass: $m_C \sim 10^3$ kg.

Fig. 6: Direct transcription control for 6DOF rendezvous: translational dynamics. TOF: $t_f = 0.8\,\mathrm{h}$. Initial relative states random.

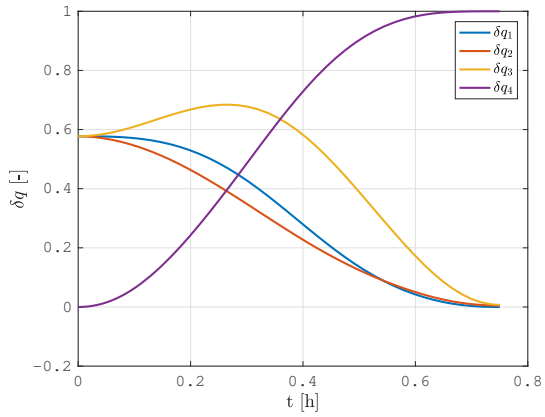

(a) Relative quaternion.

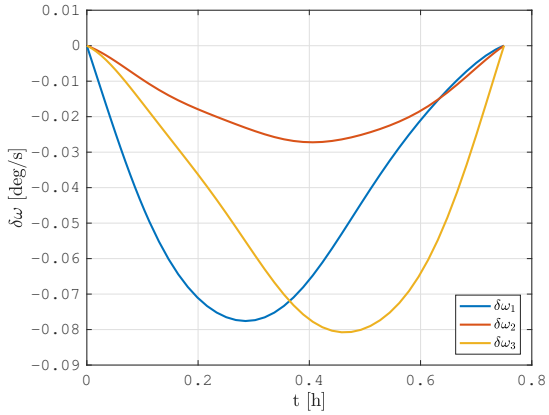

(b) Relative angular velocity.

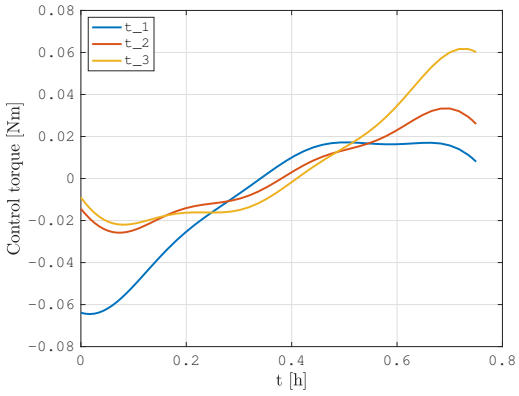

(c) Control torque. Chaser inertia moments: $\mathbb{I}_C \sim 10^4\,\mathrm{kgm}^2$.

Fig. 7: Direct transcription control for 6DOF rendezvous: rotational dynamics. TOF: $t_f = 0.8\,\mathrm{h}$. Initial relative states random.

Copyright © 2018 by Andrea Colagrossi. Published by the International Astronautical Federation with permission.

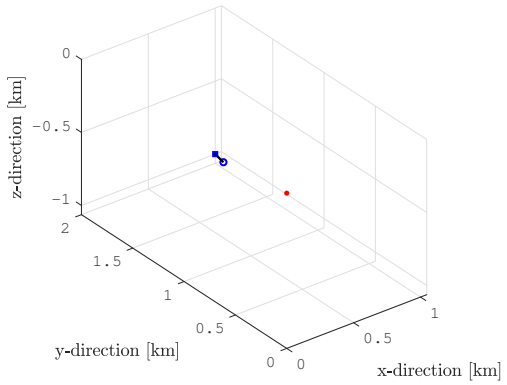

Fig. 8: Relative trajectory for the initial guess of the control parametrization, $\bar{\mathbf{p}}_0$.

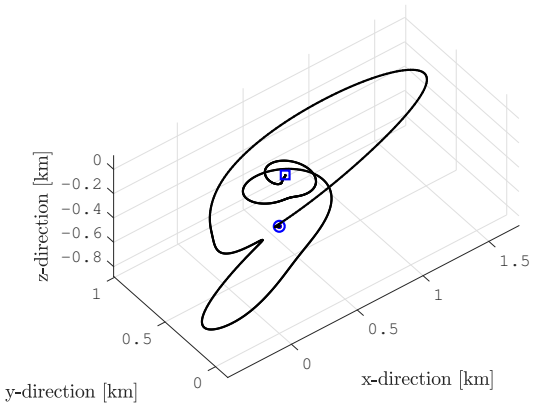

Fig. 9: Direct transcription control for a test rendezvous scenario: translational dynamics. TOF: $t_f = 10\,\mathrm{d}$.

large discontinuities in the value of the objective function and the SQP algorithm avoid to continue the minimization in that direction. An evidence, of the algorithm robustness is given in figure 8, where it is shown the relative trajectory associated with the initial guess in the control parametrization of the example case reported in figures 6 and 7.

The relative attitude dynamics control has good convergence properties if the constraints on the final relative quaternion is not enforce in vectorial form, but in scalar form. Therefore, the boundary condition on the final relative quaternion is expressed as:

$$\delta q_4^2(t_f) - 1 = 0. \tag{48}$$

As a final remark, the direct transcription is capable to solve also very complex and long rendezvous problems. They are not very useful for practical application, but they can be of interest to test the performances of the developed method. An example scenario is shown in figure 9, where an extremely long and cost effective rendezvous scenario on a L1 Halo orbit is simulated. The control optimality is guaranteed from its linear evolution, analogous to the one available from the indirect methods. However, the direct method provided the solution in a very short time and without any analytical effort.

3.3 Exploitation of natural dynamics

Natural dynamics in cislunar space, under the influence of the non-Keplerian environment, is of great interest because of the dynamical properties that can be exploited to execute transfer and rendezvous trajectories with an extremely limited control cost. The study of natural dynamics (i.e. invariant manifolds) in the three-body environments is very well known from many literature studies: as a matter of fact, stable and unstable invariant manifolds ensure affordable and robust approaching and departure trajectories from most periodic orbits in cislunar space.

In the applications discussed here, the interest is directed towards 6DOF natural dynamics. According to a previous work of the authors [11], the coupled orbit-attitude dynamics in cislunar-space allows to compute invariant orbit-attitude manifolds. They are of particular interest in the relative dynamics during a rendezvous phase. In fact, the natural orbit-attitude trajectories can be exploited to easily guide the chaser during its approach to the operational orbit of the target. The advantage of exploiting manifolds to design rendezvous operations is related to the fact that since they are associated to natural dynamics, they require negligible control action.

This research work focuses its attention in connecting the previously discussed controlled trajectories with a final natural drift rendezvous path. In figure 10 is shown the 6DOF relative dynamics on a stable manifold approaching the orbit-attitude state of the target in vicinity of the apocentre region of a L1 NRHO orbit. Figure 10a shows the classical manifold trajectories approaching to the target orbit. The relative dynamics is of great interest: the relative trajectories in figure 10b have a spiral motion toward the target that naturally bring the chaser at close distance from the docking point ($\sim 1km$). An extremely light active control action is needed to maintain the chaser on the desired trajectory and to finalize the rendezvous. During the rendezvous operations, the natural trajectory can be approached with the active control described before, which is driving the chaser up to the matching points (i.e. black dots in figure 10b), at a distance of ($\sim 50km$) from the target. Then, the rendezvous maneuver can be completed with a gentle close-loop control over the natural rendezvous tra-

Copyright © 2018 by Andrea Colagrossi. Published by the International Astronautical Federation with permission.

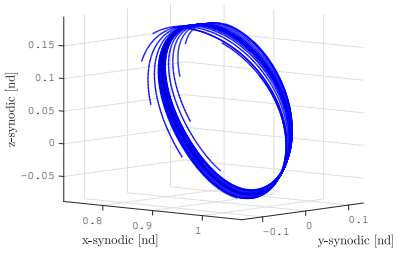

(a) Absolute translational dynamics.

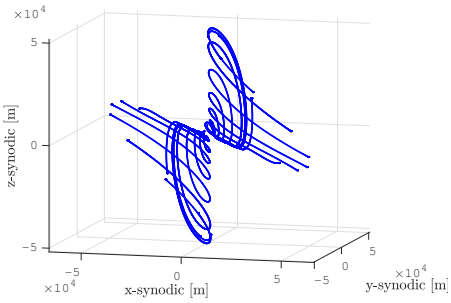

(b) Relative translational dynamics.

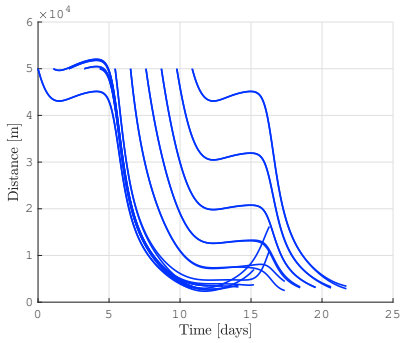

(c) Relative distance.

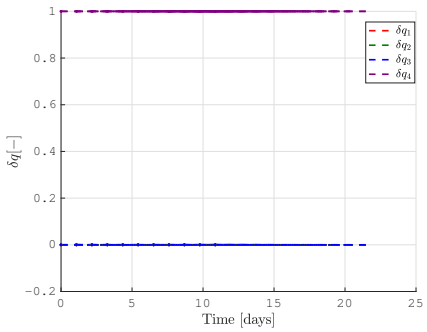

(d) Relative attitude dynamics.

Fig. 10: Stable manifold 6DOF dynamics (i.e. approach) on a L1 NRHO orbit.

jectory. This is needed just to correct eventual navigation errors, perturbations and injection inaccuracies. However, the most interesting result is reported in figure 10d: the attitude dynamics over a manifold is matched with the one of the target (note that this is true both for unstable and stable manifolds). In practice, 6DOF manifolds have no relative attitude component: the chaser can be controlled to have a zero relative attitude with respect to the target at the matching point. Then, it will naturally have an absolute attitude dynamics that is continuously matching the target attitude motion up to the docking point, when the two spacecraft will be correctly oriented, naturally. For this reason, as anticipated before, the final relative attitude boundary conditions previously discussed (i.e. zero relative attitude states at t_f) are relevant also for practical applications.

Finally, it is important to remark that for NRHOs this discussion is valid if the rendezvous point is far from the pericentre of the orbit. In fact, at the pericentre of a NRHO, the large gravity gradient torque of the Moon creates a strong perturbations on the attitude dynamics and the relative motions start drifting away very rapidly. This effect can be understood looking at figure 10c: the chaser is passing at the pericentre when there are steep variations in the relative distance. Hence, as highlighted also in previous literature studies [4, 12], rendezvous in NRHOs must be performed in the region close to the apocentre of the orbit.

4. Cislunar Rendezvous and docking operations

The methods and techniques discussed in this research work, to solve the 6DOF guidance and control problem during cislunar rendezvous and docking, have been developed having in mind practical applications and operations. From the available results, it is evident how much is important to take into account the coupled 6DOF relative dynamics for non-Keplerian orbit GNC design. Furthermore, practical operations and realistic mission scenarios have to consider many other aspects, such as safety of the manoeuvres, navigation performances and system constraints, among the others. In this section, a practical case study of rendezvous and docking operations in cislunar NRHOs is briefly discussed, together with the associated functional and performance GNC requirements [3].

4.1 Example operations results

The target is assumed in motion on a L2 South NRHO, with an orbital period of $\sim 7\,\mathrm{d}$, an apocentre distance from the lunar surface of $\sim 7 \times 10^4\,\mathrm{km}$ and a pericentre distance of $\sim 4 \times 10^3\,\mathrm{km}$. The target is moving with a orbit-attitude periodic motion as described by the authors in [4]. This peculiar target orbit-attitude dynamics is characterized by: large difference in orbit-attitude velocities

Copyright © 2018 by Andrea Colagrossi. Published by the International Astronautical Federation with permission.

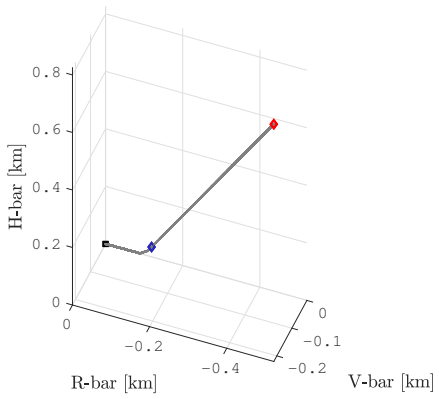

(a) Rendezvous in relative LVLH frame.

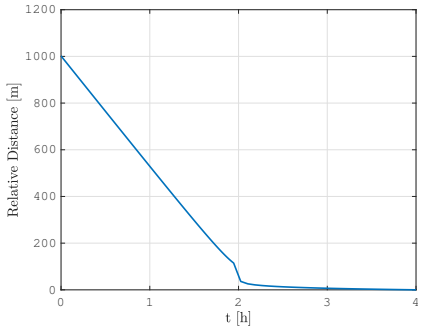

(b) Relative distance.

Fig. 11: Rendezvous trajectory from the holding point HP, (red diamond), to docking, (black dot). Alignment with the docking port axis at a distance of $\sim 100\,\mathrm{m}$ (blue diamond).

between pericentre and apocentre, and symmetry with respect to the $\hat{X} - \hat{Z}$ plane. This orbit has been selected as settings for this example rendezvous scenario because an eventual space station in cislunar space will be probably staged on an orbit of this kind. This selection can be explained because NRHOs are, among other advantageous characteristics, always visible from Earth and they have long visibility windows over lunar south pole [2].

The rendezvous operations, to go from a generic position in space up to the docking conditions with the target, are characterized by the following requirements:

- ◇ Final rendezvous and docking shall be performed in proximity of the apocentre of the selected NRHO ($\pm 50°$ of mean anomaly);
- ◇ The overall rendezvous trajectory shall be optimised to minimise the total control energy;
- ◇ The rendezvous trajectory shall pass through a designed holding point, HP;
- ◇ The holding point HP shall lie on the central manifold of the NRHO. This allows, in case of misfiring or no firing at all, to remain at about $\sim 1\,\mathrm{km}$ from the target, without getting in closer proximity inside the $1\,\mathrm{km}$ keep-out-sphere (KOS). In order to have subsequent opportunities to perform the transfer or to perform abort/contingency manoeuvres. Note that, since the manifolds of the NRHO change in time, the rendezvous analysis is strictly coupled with the phasing trajectory analysis [12, 13];
- ◇ The docking alignment path point shall lie on the negative R-bar direction, at $\sim 100\,\mathrm{m}$ from the target;
- ◇ Passive safety shall be ensured at all times;
- ◇ Active safety collision avoidance manoeuvre shall be designed as backwards rendezvous trajectories;
- ◇ The navigation cameras and the docking port shall be mounted with an angular offset of $90°$ in chaser body frame. Hence, the rendezvous trajectory has to perform a proper rotation: to align the docking port at $t = t_f$ and to maintain the target in the camera field of view. This rotation is performed between the holding point, HP, passage and the docking alignment path point.

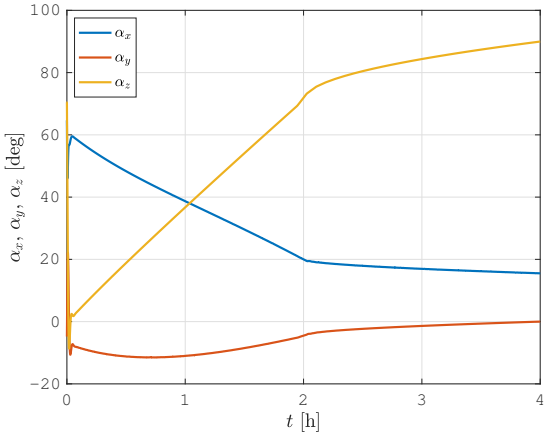

Fig. 12: Attitude rendezvous trajectory from the holding point HP. Absolute attitude dynamics of the chaser, expressed in Euler $XYZ-$angles with respect to the inertial frame I.

The rendezvous example discussed here, since its operative implementation purpose, is represented in the target centred relative LVLH frame, as defined in [5], and with

Copyright © 2018 by Andrea Colagrossi. Published by the International Astronautical Federation with permission.

absolute Euler $XYZ-$angles with respect to the inertial frame I.

The initial rendezvous point for the simulated application of the developed guidance and control algorithms is on the holding point HP at the border of the KOS. The actual arrival to the holding point is not addressed in this paper. However, the point HP can be approached: with another energy optimal rendezvous trajectory, with a slightly controlled natural drift on the stable manifold, or with a classical impulsive manoeuvre trajectory. As per requirements, the holding point HP lies on the surface of the KOS on the central manifold direction.

The final docking approach is designed to occur from the negative R-bar direction to bring the chaser at the docking port, as in figure 11a. The control trajectory has been designed imposing the passage through a docking alignment path point (blue diamond in figure 11a), in order to connect the holding point HP with the imposed path constraints. In fact, in this example, the direct transcription control moves the chaser away from HP and brings it progressively at the docking alignment point: positioned at $\sim 100\,\mathrm{m}$ from the target, on the unstable manifold approach corridor, mainly aligned with the R-bar direction. The forced translation is maintained within a cone approach corridor defined by the NRHO unstable manifold, again, for passive safety enforcement. In fact, in case of problems in the control functions, the unstable manifold guarantees a safe drift away from the target, but the time scale is slow enough to allow recovery of the nominal operations. Then, from the docking alignment point to the final rendezvous point, the control produces a straight trajectory along the R-bar direction. The relative distance reduction during this last phase is very slow, as in figure 11b, for safety reasons. The required Δv to perform this rendezvous phase is: $\Delta v \simeq 0.32\,\mathrm{m/s}$.

In figure 12 the absolute attitude of the chaser is reported during the rendezvous phases. The chaser has to rotate of approximately 55° around one axis to align the docking port and to maintain the target in the supposed camera field of view. In fact, while approaching from HP, the chaser is reducing its H-bar distance with respect to the target and a rotation is necessary to maintain the desired alignment. After the docking alignment point, the motion is almost only along R-bar and, therefore, the attitude dynamics is almost coincident with the target nominal periodic attitude [4]. The attitude guidance profile is obtained with the developed direct transcription methods, to minimize the required control energy. The simulation in figure 12 is initialized from a random attitude state and, hence, the control function first achieves the optimal attitude profile, then maintains the chaser on the desired path.

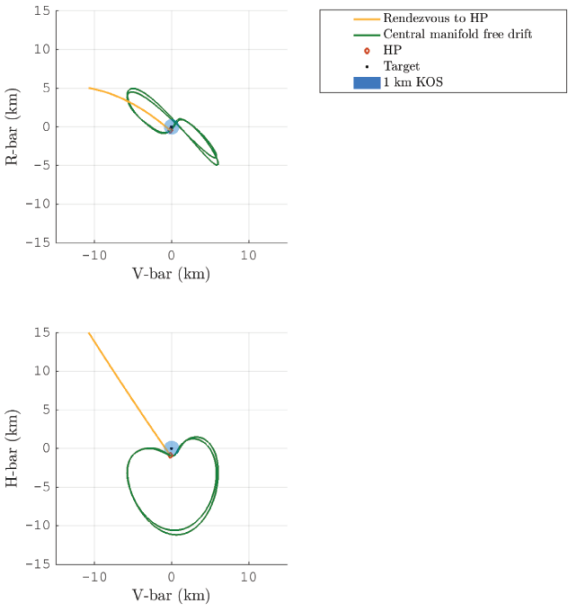

Fig. 13: HP position in relative LVLH with holding point on the central manifold of the NRHO and following free drift trajectory simulated for 2 NRHO periods.

4.2 Passive safety

Passive safety shall be enforced at all times and, to satisfy this requirement, the rendezvous trajectory has been designed exploiting the features of the relative 6DOF dynamics in cislunar environment. This possibility is allowed by the proposed direct transcription control, through a proper selection of the constraints verified with the numerical simulation of the relative non-Keplerian dynamics.

The holding point (i.e. HP) settling on the central manifold entails that, if the control function is not working and the rendezvous manoeuvres are not performed, the chaser remains hovering around the target with a periodic motion. In figure 13, the chaser is naturally hovering in proximity of the $1\,\mathrm{km}$ KOS, with enough time to have the control system working back again. In this case, weak passive safety is enforced. If strong passive safety is sought, as inside the KOS, the path points must be designed on the unstable manifold corridor, which guarantees natural drift away from the target if a problem occurs.

4.3 Active safety

Contingency operations can be managed exploiting active safety enforcement and, in particular, Collision Avoidance Manoeuvres (CAMs) are planned, to have the chaser with minimal collision risk with the target when a prob-

Copyright © 2018 by Andrea Colagrossi. Published by the International Astronautical Federation with permission.

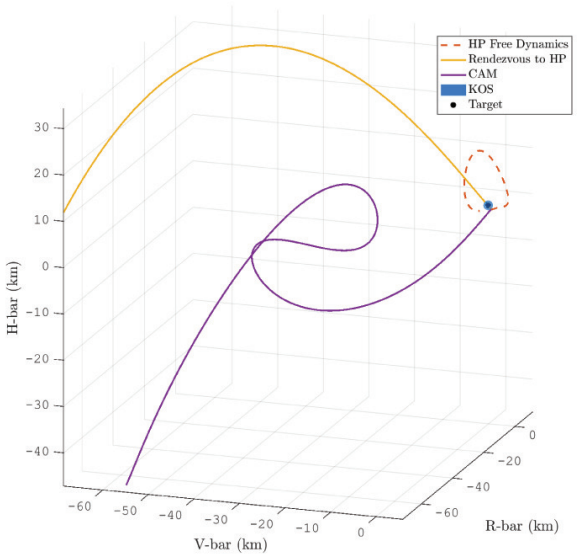

Fig. 14: Active safety: CAM manoeuvre from HP.

lem occurs. Collision avoidance manoeuvres are to be intended in addition to nominal passive safety enforcement at all times of the rendezvous and docking operations. If a non-nominal condition occurs, the chaser, after the CAM execution, is retreated to a safe hold point.

The CAMs can be computed with the direct transcription control method, setting a safe 6DOF relative state as a final boundary condition for the algorithm. The CAMs can be designed from any point along the rendezvous trajectories to any safe holding point. In figure 14, an example CAM trajectory is shown. The TOF is imposed to be twice the nominal rendezvous time, in a way that no large control action is required. Thus, assuming that the system is undergoing non-nominal operations, in the worse case scenario, even a wrongly commanded CAM manoeuvre can be recovered.

5. Final Remarks

Rendezvous and docking control techniques presented and analysed in this paper are an example of GC functions for transfer operations in the Earth-Moon system. The future space missions that are proposed to stage a space station in cislunar environment require a careful planning of all the rendezvous operations and, due to the dimensions of the space system itself, the attitude coupling is of primary relevance; in particular, when considering relative dynamics.

Extensive knowledge of orbit-attitude relative dynamics in cislunar space is fundamental to design proper GC functions and to leverage coupled natural dynamics in helping the rendezvous design process. Further investigations are needed to extend the range of these preliminary results. In particular, passive dual-spin attitude stabilisation methods, analysed by the authors in recent works (e.g. [10]), can be integrated with the currently proposed active attitude control system. Moreover, a careful investigation of the entire cislunar space environment can extend the range of selection for the nominal staging orbit. For example, an orbit with a higher pericentre altitude can be helpful to extend the available time window to perform rendezvous operations.

Recent research works of the authors, which include the research presented in this paper, were carried out to emphasise the importance in studying the fully coupled orbit-attitude dynamics while designing the architecture to build and operate a large and modular space structure in cislunar orbits. The coupling with the structural flexibility is another important aspect in this research framework. Future studies will take back again in consideration the structural dynamics of extended space infrastructures, which could be excited by the active control system and, thus, it could generate non-nominal situations during rendezvous and docking phases.

References

[1] International Space Exploration Coordination Group (ISECG), “The global exploration roadmap”, 2018.

[2] R. Whitley and R. Martinez, “Options for staging orbits in cislunar space”, in *2016 IEEE Aerospace Conference*, 2016.

[3] L. Bucci, A. Colagrossi, and M. Lavagna, “Rendezvous in lunar near rectilinear halo orbits”, *Advances in Astronautics Science and Technology (Online First)*, 2018. DOI: 10.1007/s42423-018-0012-6.

[4] A. Colagrossi and M. Lavagna, “Preliminary results on the dynamics of large and flexible space structures in halo orbits”, *Acta Astronautica*, vol. 134, pp. 355–367, 2017.

[5] ——, “Dynamical analysis of rendezvous and docking with very large space infrastructures in non-keplerian orbits”, *CEAS Space Journal*, vol. 10, no. 1, pp. 87–99, 2018.

[6] M. J. Sidi, *Spacecraft Dynamics and Control: A Practical Engineering Approach*. Cambridge University Press, 2000.

Copyright © 2018 by Andrea Colagrossi. Published by the International Astronautical Federation with permission.

[7] J. R. Wertz, *Spacecraft Attitude Determination and Control*. Kluwer Academic Publishers, Dordrecht, 1990.

[8] G. Q. Xing and S. A. Parvez, "Alternate forms of relative attitude kinematics and dynamics equations", in *2001 Flight Mechanics Symposium*, 2001.

[9] R. J. Luquette, "Nonlinear control design techniques for precision formation flying at lagrange points", PhD thesis, University of Maryland, College Park, 2006.

[10] A. Colagrossi and M. Lavagna, "Dynamics and control of modular and extended space structures in cislunar environment", in *26th International Symposium on Space Flight Dynamics*, 2017.

[11] ——, "Assembly and operations for a cislunar orbit space station", in *68th International Astronautical Congress*, 2017.

[12] L. Bucci, M. Lavagna, and F. Renk, "Relative dynamics analysis and rendezvous techniques for lunar near rectilinear halo orbits", in *68th International Astronautical Congress*, 2017.

[13] ——, "Phasing and rendezvous operations on non-keplerian orbits in the earth-moon system", in *69th International Astronautical Congress*, 2018.